ACS APPLIED MATERIALS & INTERFACES

Research Article

www.acsami.org

Nanoscale Hydrophilicity Studies of Gulf Parrotfish (*Scarus persicus*) Scales

Abigail Plummer,[‡,§] Tzu-Chieh Tang,[†,§,∥] Chia-Yun Lai,[†] and Matteo Chiesa*[,†]

[†]Laboratory for Energy and NanoScience (LENS), Institute Center for Future Energy (iFES), Masdar Institute of Science and Technology, P.O. Box 54224, Abu Dhabi, United Arab Emirates

[‡]Department of Physics, Brown University, Providence, Rhode Island 02912, United States

Supporting Information

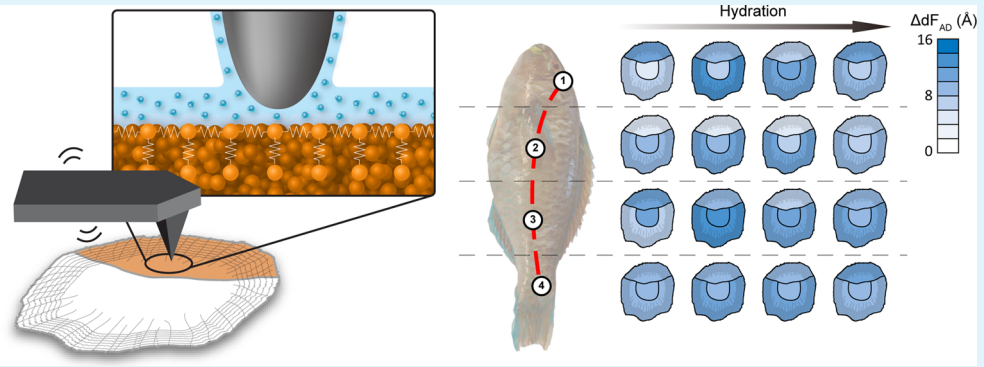

ABSTRACT: The Gulf parrotfish (*Scarus persicus*) offers inspiration for a strategy to combat marine biofouling, a problem of great economic and environmental interest to the maritime community, through its use of a continually maintained, multifunctional, water-based mucus layer to cover its scales. In this study, to better understand the scale−mucus interface, we investigate the nanoscale hydrophilicity of the fish scales by comparing reconstructed force distance profiles obtained using an amplitude-modulation atomic force microscopy (AM-AFM) technique. We note significant differences between three morphologically distinct regions of each scale, as well as between scales from four spatially distinct regions of the fish. This study reveals a previously unreported property of fish scales and proves the value of a new AFM technique to the field of biomaterials.

KEYWORDS: *fish scale, wetting, adsorption, contact angle, AFM*

INTRODUCTION

As science increasingly looks to nature for inspiration for novel materials,[1] the external surfaces of marine life have attracted much attention for their ability to provide clean, flexible, hydrodynamic, and lightweight protection.[2] These properties hold great appeal for those looking to create flexible armors[3] and antifouling surfaces, especially for nautical vessel applications.[4] Studies on shark skin,[5] clam shells,[6] and fish skin[7] have sought to understand and replicate these properties, and some have even already yielded commercial applications. Boats in particular have much to gain from this work, because significant savings could be achieved if hydrodynamic efficiency and durability of materials were increased.

Fish scales provide a particularly inspiring system for this kind of study. Made of rigid overlapping discs, the covering has been reported to have a strain-rate dependence that is an order of magnitude higher than bone[8] while still assisting the fish in locomotion.[9] Moreover, while alive, these scales are covered with a layer of mucus. The high water content mixture of glycoproteins, produced by cells embedded in the fish skin, forms a continuous layer of slime around the fish that appears to have far ranging properties from ionic regulation to hydrodynamic properties to resistance to abrasion and disease.[10] This dynamic functional coating is also stable, remaining on the scales during potentially disruptive daily activities. Knowledge about the interface between the scales and the mucus layer is a critical part of understanding this system, and because the mucus is water-based, hydrophilicity studies of scales are an important element of this work. If successfully applied to nautical vessels, fish mucus principles could improve fuel efficiency and material properties and could open up a new class of biodegradable and resilient functional coatings.

There have been a number of studies on the mechanical[2,7,9,11] and hydrodynamic properties[12] of fish scales. These studies have reported that the multilayer structure of the scale makes it remarkably resistant to penetration[7] with a high tensile strength[13] and good fracture toughness, but many also note that these properties are significantly affected by whether the scale is in the hydrated or dry state.[8] Surprisingly, there have been very few efforts to characterize the changes that a scale

Received: July 13, 2014
Accepted: September 2, 2014
Published: September 2, 2014

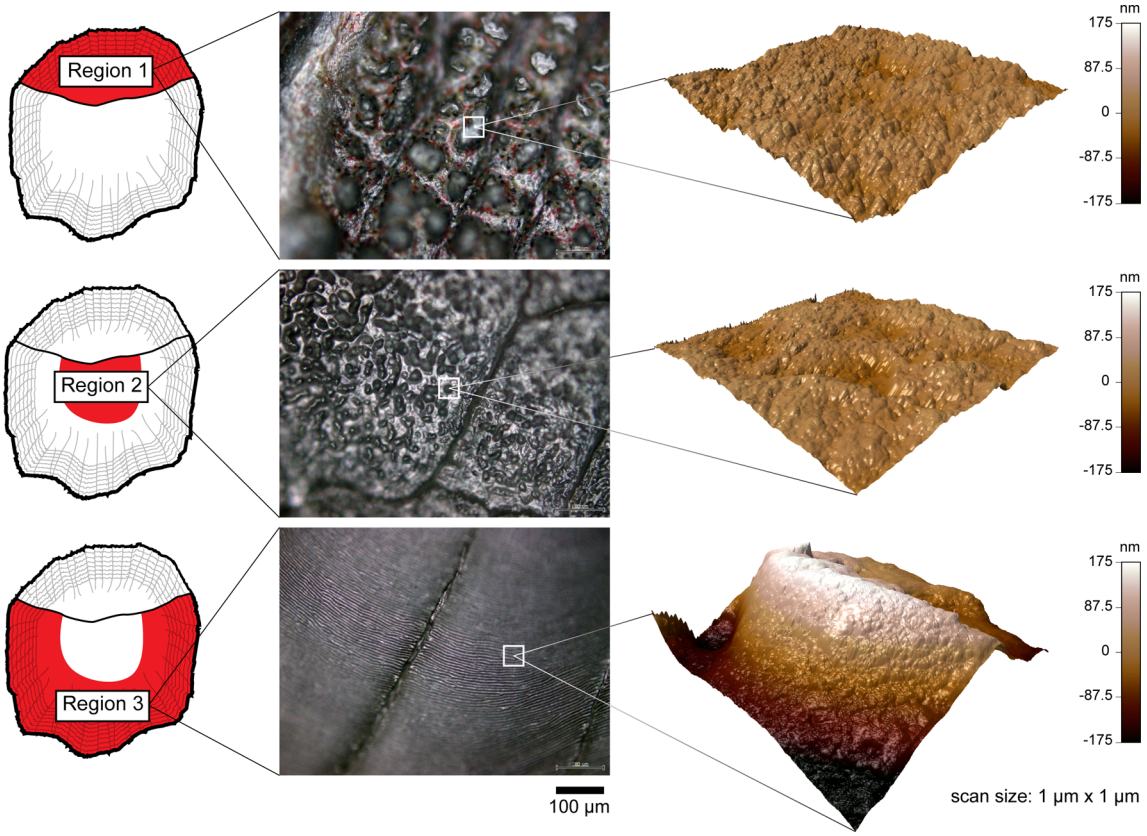

Figure 1. (Left to right) diagrams indicating the three regions (red) on a scale, optical microscope images, and AFM images of each distinct region.

undergoes when exposed to moisture, despite the attention given to the difference between the dry and hydrated state in literature. This understanding is required to enable further studies about scale−mucus interactions as well as fish−ecosystem interactions.

One way to characterize this key wetting behavior is through contact angle measurements. In fact, this is one of the most common tests used to characterize biomaterials[14] because of the relevance of hydrophobicity for applications such as desalination, drag reduction, and self-cleaning materials. However, contact angle measurements have inherent limitations that make them unsuitable for characterizing many biomaterials. First, the minimum drop size required for normal contact angle measurement is too large to be able to accurately probe different regions of a typical fish scale, particularly if the scale is not hydrophobic. For fish scales in particular, variance in properties because of the degree of hydration make these measurements difficult to repeat.[8] Second, the measurements can be unreliable due to small surface irregularities.[15] Finally, contact angles only shed light on the macroscopic interaction between a material and water. Environmental scanning electron microscopy (ESEM) provides an alternative solution, allowing the observation of wetting behavior of hydrated samples at the scale of a few microns. Unfortunately, the contact angle obtained from ESEM is still prone to the limitations of traditional measuring methods. Although this information is valuable, the nanoscale structure of many biomaterials demands a method of characterizing hydrophobicity that can operate with nanoscale resolution.

In this research, we have investigated the differences between fish scales of the Gulf parrotfish, *Scarus persicus*, under four conditions using a force reconstruction technique based on atomic force microscopy (AFM). The scales were examined first in standard laboratory conditions (40% < RH < 50%), and then they were placed in a high humidity environment (RH > 90%) and tested twice more, once after 30 min and again after 1 h. Finally, the scale was examined after 1 μL of deionized water was placed on the region and allowed to absorb into the scale. This is defined as the hydrated state.

Here, results are presented that show that there are significant differences in how the water layer develops on different regions of a single scale and on different scales on a single fish. The results also suggest that the force reconstruction method detailed here holds great promise for future characterization of nanoscale water affinity for complex systems. This application of physical principles allows biological researchers to probe the nanoscale with a new and powerful tool.[16]

EXPERIMENTAL SECTION

Fish Sample Preparation. The parrotfish used in this study were obtained fresh from a local supplier. Multiple scales were extracted from various regions of interest, washed with Milli-Q water using a pipet repeatedly, immersed in stirred Milli-Q water, blown dry with 99.9% pure nitrogen gas, and refrigerated in a sealed container. Subsequent AFM scans showing clean surfaces without biofilms confirm that this cleaning protocol is sufficient. Three 2 × 2 mm squares were cut from the center of each region on each scale and fixed to metal discs using epoxy.

ESEM. A Quanta 250 ESEM microscope was employed for surface wettability investigations. Samples of the scales, 2 × 2 mm each, were cut from each region of interest, mounted on the sample holder, and placed on the cooling stage. The stage was maintained at 0 °C, and the ESEM chamber was maintained at 100 Pa for 20 min, allowing scales to cool. The pressure was then increased to 700 Pa to create water droplet condensation. The ESEM was operated at an electron

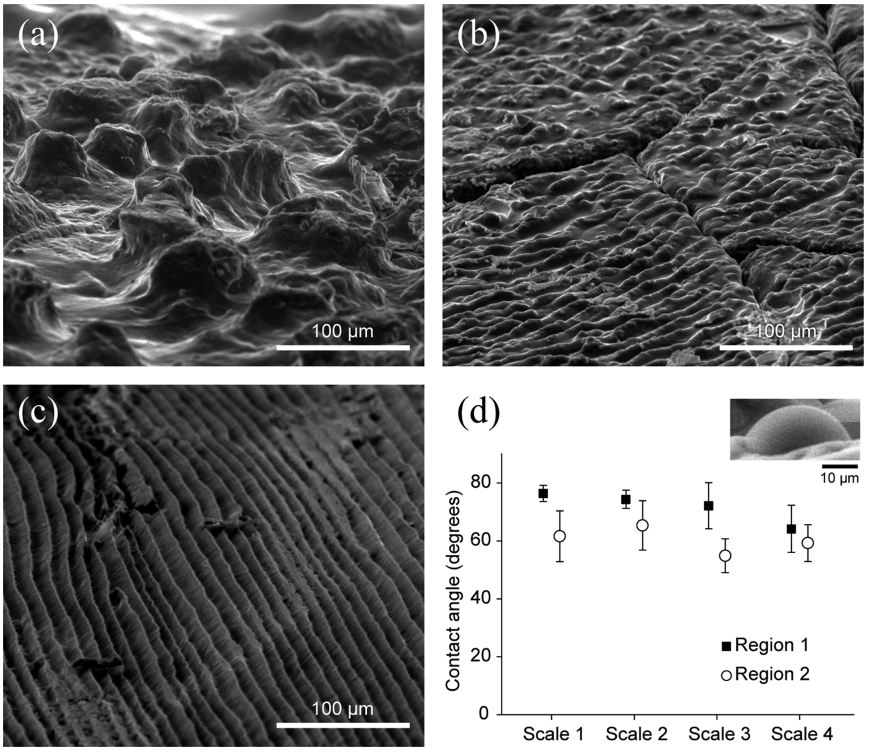

Figure 2. Environmental scanning electron microscopy (ESEM) images of a fish scale at (a) Region 1, (b) Region 2, and (c) Region 3. (d) The contact angles measured on different scales along the fish's anteroposterior axis. Statistics refers to 14 droplets measurements for each region. (Inset) A typical droplet from Region 1.

accelerating voltage of 15 kV. Videos were recorded when water condensation was taking place. Images were then processed with ImageJ software for water contact angle analysis.

AFM. AFM images were acquired using an Asylum Research Cypher Scanning Probe Microscope and OLYMPUS AC160TS tips (spring constant, k ≈ 40 N/m; quality factor, Q ≈ 500; resonance frequency, f = f_0 ≈ 300 kHz; and tip radius, R ≈ 7 nm) in noncontact mode. During scanning, we operated at a free amplitude of 4 nm and a set point of 3 nm. The resolution of images was 512 × 512 pixels over a 1 × 1 μm area, and the scan rate was 0.5 Hz.

Force Reconstruction. The amplitude-phase-deflection (APD) curves of selected regions (Figure 1) were taken with a Cypher and OLYMPUS AC160TS tips. We employed amplitude modulation AFM (AM-AFM), a technique in which the driving frequency of the AFM cantilever is kept constant, and experimental values for the differences in amplitude, phase, and deflection as the tip approaches the sample are obtained. The APD curves were then used for force reconstruction with a recently developed technique[17] based on the Sader–Jarvis[18]–Katan[19] formalism (eq 1), which allows us to use the curves to approximate the cantilever as a driven damped harmonic oscillator and reconstruct the conservative forces acting on the tip as a function of tip–sample separation for the point that was approached on the sample. In this formalism, the tip–sample force, F_{ts}, versus minimum distance of approach, d_m, is recovered from variations in the frequency shift, Ω, that result from decreasing the cantilever-sample separation, z_c. The cantilever-surface separation z_c can relate d_m, or equivalently d, to the oscillation amplitude A ($d_m \equiv d \approx z_c - A$) (Figure 2a). Then, the normalized conservative force F_{ts}^* is[18]

$$F_{ts}^*(d) = \frac{2k}{|F_{AD}|}\int_{u=d}^{u=\infty}\left[\left(1+\frac{A^{1/2}(u)}{8\sqrt{\pi(u-d)}}\right)\Omega(u) - \frac{A^{3/2}(u)}{\sqrt{2(u-d)}}\frac{d\Omega(u)}{du}\right]du \quad (1)$$

In eq 1, k is the spring constant of the tip while A is the amplitude of oscillation. For each curve, the normalization is carried out with the absolute value of the minimum of force (force of adhesion, F_{AD}, which is defined experimentally) and where Ω is the normalized frequency shift expressed by

$$\Omega(d) = \left[1+\frac{A_0}{QA}\cos(\Phi(d))\right]^{1/2} - 1 \quad (2)$$

In eq 2, A_0 is the free amplitude of oscillation, while Φ is the phase lag relative to the drive force. However, this reconstruction is not necessarily complete due to dissipative forces acting on the cantilever as well as a region of bistability and discontinuity during the tip approach cycle in which two distinct tip–sample separations are solutions to the force reconstruction equations. In order for us to recover the whole range of d, A_0 needs to be finely controlled. Thus, we operated at free amplitude (A_0) ≈ 40 nm and trigger point ≈ 36 nm, respectively. This relatively high set point enables us to avoid the bistability between the attractive and repulsive region in the APD curves during cantilever approach and instead yields a smooth transition between the two regimes.[20,21] To avoid tip blunting and contamination, we constantly monitored the tip radius, R, in situ by using the A_C method,[22] which measures the critical amplitude where the transition from the attractive to the repulsive regime occurs. Moreover, peak forces can be tuned by carefully selecting the minimum reduction in amplitude (for example, 90% of A_0, which is 36 nm) in order to reduce invasiveness on sample and area of interaction.[23−25]

Ultrahigh resolution characterization techniques inherently risk accidentally focusing on aberrations rather than representative areas. In order to mitigate this risk in our study, we have carefully used lower resolution AFM scanning to decide where to approach the sample, constantly monitored the tip radius to ensure it did not become contaminated, and checked that observed trends were present in multiple fish.

RESULTS AND DISCUSSION

Parrotfish have cycloid scales that, like most modern fish, have a thin bony layer composed of calcium-deficient hydroxyapatite deposited in concentric rings as the fish grows, covering a thicker, more flexible collagen layer. This structure has been observed by a number of groups.[2,7,8] The difference in the absorptiveness of the two layers can be observed in a dry fish scale. The scale has a tendency to curl tightly along the longitudinal axis with the bony layer facing outward. When hydrated, the underlying collagen layer absorbs water and once again expands, flattening the scale. Unfortunately, in this study we were only able to examine the scale's hydration reaction to Milli-Q water. Further studies could investigate how the reaction may differ when a material closer in composition to the fish's natural mucus is used to hydrate the scale. Again, as this mucus is known to have a high water content, Milli-Q hydration is a reasonable approximation to mucus hydration.

Preliminary optical microscope scans on unfixed scales allowed us to define three distinct regions within the scale (Figure 1, middle column). Region 1 is defined as the portion of the scale that is exposed to water. Visually, this region is darker than the others due to the pigment cells that lie on its underside. Morphologically, this area is covered in microscale pillars. Region 2 can be identified as the region in the middle of the scale where small ridges form serpentine and irregular patterns. Region 3 is the border of the scale, composed of ridges that are similar to those in Region 2 but are instead smaller and organized into regular concentric bands that intersect with the scale radii. It is in this region where new growth occurs, and small hydroxyapatite crystals are visible on the tops of the ridges with an optical microscope. AFM images allow us to further examine the detailed morphological difference between regions. As shown in Figure 1, topographical scans were taken from the pillars in Region 1 and the ridges in Regions 2 and 3. The nanoscale surface roughness of the three regions as measured by AFM are 13.50 ± 3.38, 12.08 ± 1.96, and 20.84 ± 5.70 nm, respectively.

The ESEM images enable us to examine the different regions in more detail. In Region 1 (Figure 2a), the pillars are positioned ~100 μm apart from each other with individual height of ~50 μm. This feature contributes to the difficulties in obtaining contact angle by traditional methods as droplets become stretched and cannot maintain symmetric shapes. Region 2 (Figure 2b) exhibits small bumps (<10 μm in height) arranged in rows, marking the transition between Regions 1 and 3 (Figure 2c). The condensation of water droplets on these surfaces can be studied by increasing the relative humidity in the chamber.[26,27] Region 1 is slightly more hydrophobic than Region 2, based on contact angle measurements with droplet sizes of ~30 μm (Figure 2d). However, the contact angles vary widely and cannot be measured in Region 3 due to drastic variation in topography (Video S1, Supporting Information), which indicates that a method other than contact angle measurements with higher resolution is required to study the wetting behavior of rough and hydrophilic biological samples. On the other hand, force reconstruction with AFM has demonstrated its ability in probing wettability at the nanoscale, unaffected by surface roughness, making it suitable for our current study.[17,28]

To establish a systematic understanding of the hydrophilicity on the parrotfish surface, four representative districts were selected. The scale districts focused on in this report are (1) on top of the head, (2) underneath the pectoral fin, (3) a representative body scale, and (4) close to the tail. All four scale regions lie along the fish's anteroposterior axis (Figure 5a).

A cantilever oscillates over the fish scale with a user's prescribed oscillation amplitude A and frequency f_0 (Figure 3a). As the tip approaches the surface, amplitude, phase, and deflection versus distance, d, are recorded and used for force reconstruction (Figure 3b; see also the Experimental Section). Two typical reconstructed force profiles of tip-scale interaction are presented in Figure 4. When analyzing the force profiles, two cropping values were selected: 5% of the normalized force of adhesion (F_{ts}^*) at the larger distance value and 80% of F_{ts}^* at the smaller distance value. The distance between these two points is defined as ΔdF_{AD}, and is used as an easily quantifiable fingerprint of the force profiles. The 80% leftmost cutoff was selected in order to exclude the effect of the elastic modulus of the material (related to the slope of the linear region at small separation distances). Although it has been reported that the elastic modulus is also related to the state of scale hydration,[3] the authors considered this beyond the scope of the current study. Using the proposed formalism, ΔdF_{AD} depends on the short-range tip−sample interaction, usually dominated by van der Waals forces controlled by the local chemistry of the material. Earlier this year,[17] it was shown that a broadening of the force distance profile corresponded to an increasingly thick water layer on the substrate. When a water layer forms, a region is created in which the force on the tip is constant despite changes in tip−sample separation as the tip probes the properties of the water layer itself rather than the surface properties of the sample.[23] This constant region creates an especially broad force profile, allowing us to correlate the width

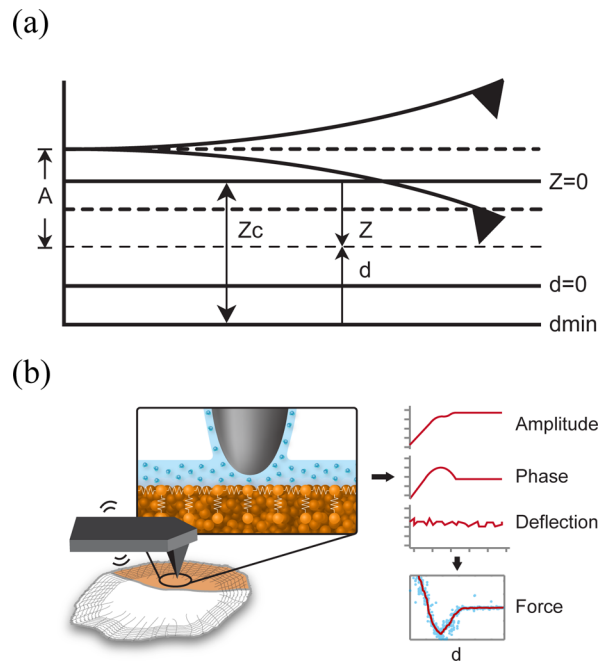

Figure 3. (a) Diagram of a cantilever vibrating over a surface with instantaneous tip position, Z, relative to unperturbed equilibrium position of the cantilever, d, and mean cantilever deflection Z = 0. (b) The process of force reconstruction. Amplitude-phase-deflection (APD) curves are obtained from the different regions on scale and processed to generate force−distance curves.

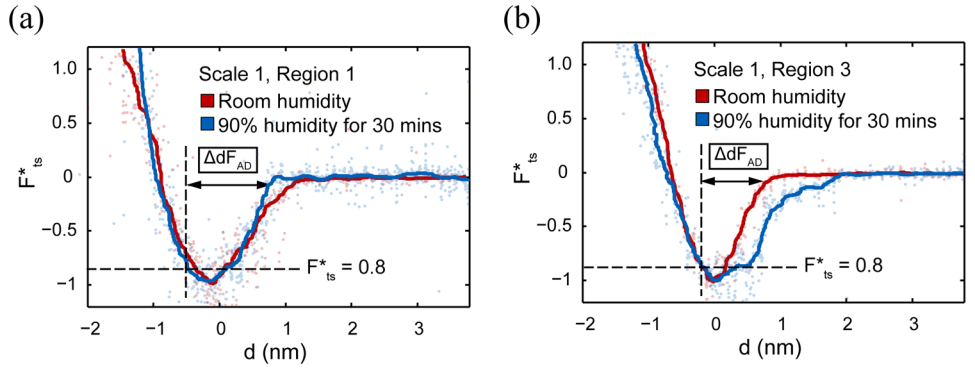

Figure 4. Normalized force profiles of a tip interaction with (a) Region 1 and (b) Region 3.

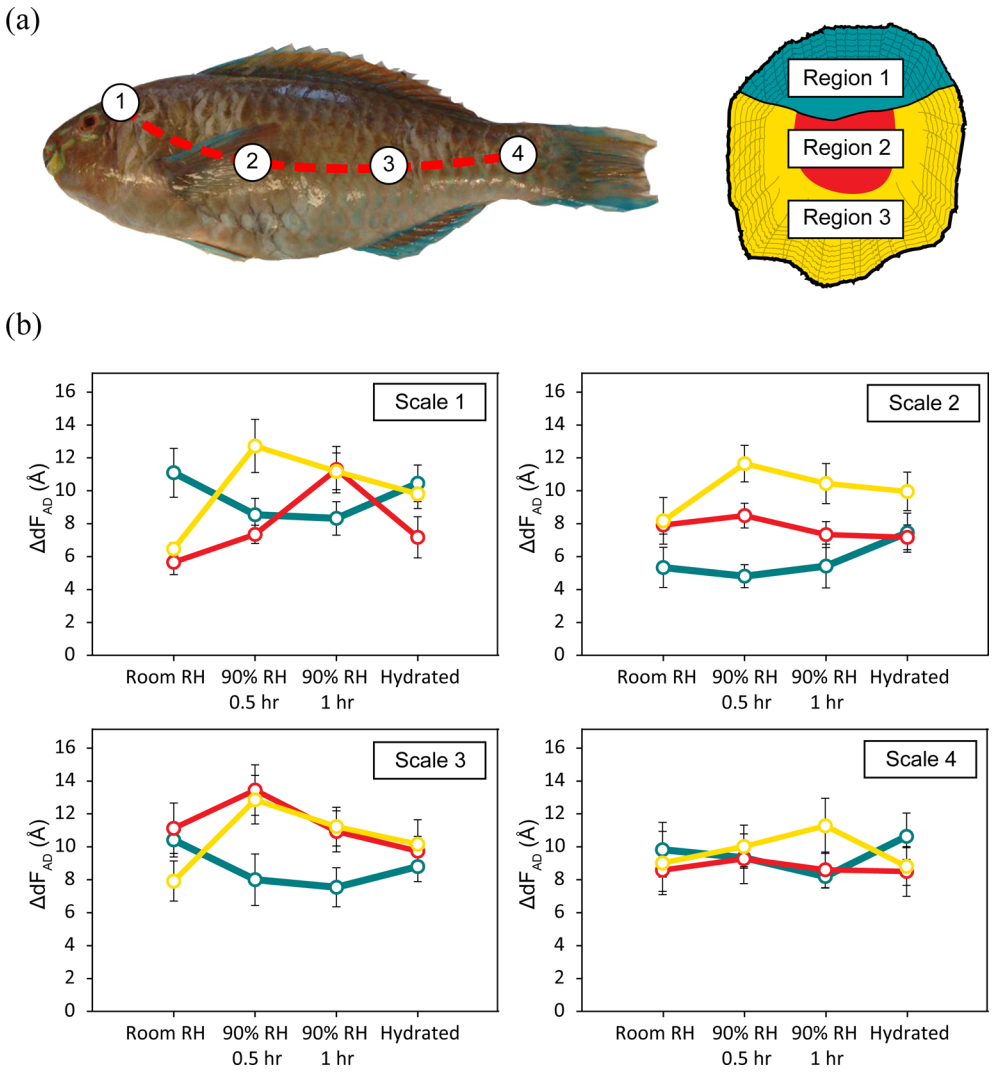

Figure 5. (a, left) Four districts from which the scales were collected and (right) the color theme of the three scale regions; (emerald) Region 1, (red) Region 2, and (yellow) Region 3. (b) The ΔdF_{AD} of each region on different scales under four conditions. Each point represents 10 curves taken at different points within a single region.

of the force profile with the thickness of the nanoscale water layer forming on the sample.

Our investigations into nanoscale water layer formation revealed that there were differences in water affinity both between regions of the scale and between scales. The clearest trend appeared when comparing the regions of each scale. The wetting behavior of Region 1 behaves inversely to that of Regions 2 and 3. We expect that this difference is related to the fact that only Region 1 naturally comes into contact with seawater.

Generalizing across scales, Regions 2 and 3 tended to form a concave down trend for ΔdF_{AD} as the degree of hydration increases along the x axis, while Region 1 forms a concave up trend, as shown in Figure 5b. Thus, the data show that for

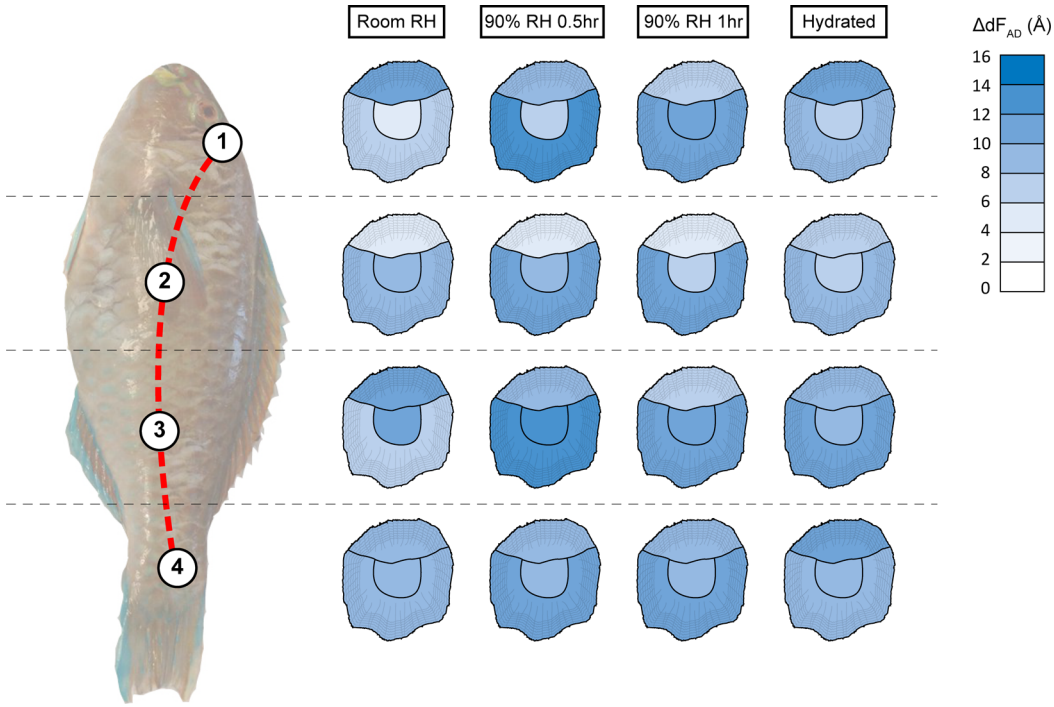

Figure 6. Hydrophilicity map of the scales at different stages of humidity treatment. (Note that the diagrams do not reflect the true scale shapes.).

Regions 2 and 3, as the relative humidity increases from room level to the fully hydrated state, the width of the profile, and thus the water layer thickness, increases rapidly at first and then begins decreasing until it nears its original level. For Region 1, the water layer thickness decreases initially under high humidity and later rises close to original levels.

As we interpret these results, the first conclusion that can be drawn is the connection between the structure of the scale region and the behavior observed under various humidity environments. Regions 2 and 3 are both made up of ridges, while Region 1 is made up of pillars. However, rather than focusing purely on the connection between form and function, it must be noted that given the nature of the AFM, this data only applies to a single point on the scale in terms of area observed and only probes the first few nanometers of the scale in terms of depth. Thus, the observed effects are related primarily to the chemistry of the scale and the intermolecular forces rather than any general microscale structures, although the authors believe the similarities between Regions 2 and 3 suggest that a study of the microstructure's relation to hydrophilicity would also produce interesting results.

Next, the framework of scale region functionality can be used to interpret the connection of behavior between scale regions. Because Region 1 is the only region exposed to the water, it has the greatest mucus retention role to play, while Regions 2 and 3 are embedded in the epidermal layer. To speculate further, because the water layers seem to be varying dramatically in thickness, it is likely that this behavior is not only related to the surface chemistry but also to the multilayer structure of the scale itself. In Regions 2 and 3, as humidity increases, the water builds on the scale until it reaches a threshold above which it is able to disappear from the view of the AFM—presumably absorbed into the underlying spongy collagen layer. In Region 1, the water seems to reach this threshold immediately, with water layer thickness decreasing with relative humidity until the third data point, which represents a saturation point (Figure 5b). These proposed mechanisms require further study to confirm and explore these suggestive trends regarding the interplay of both interlayer functionality as well as regional variation.

Trends between the scales are less clear, although our results show a number of interesting features. A color map of hydrophilicity (Figure 6) was built on the basis of the ΔdF_{AD} profiles of each scale at different humidity treatments. Using scale three, the representative body scale, as a baseline, the most noticeable differences are the shift of the peak ΔF_{AD} in scale one, Region 2, toward higher humidity, as well as the lack of significant variation between the regions on scale four. By the logic of evolution, one can reason that these variations are related to the different needs of the scales in different parts of the fish. For example, scale one requires less mucus to lubricate interscale motion, because these scales are not required to slide past one another as frequently during routine swimming. However, it may require more mucus to reduce viscous drag, because this is the part of the fish that has the most unsheltered exposure to water. Scale four, on the other hand, has much higher flexibility of motion needs that perhaps outweigh some hydrodynamic concerns. One should also note that, at a larger scale, different microstructures (bumps, pillars, ridges) at different regions on different scales also take parts in the overall mucus retaining mechanism. On the basis of the fundamental understandings at the nanoscale reported in this study, we might be able to systematically investigate the complicated mucus−scale interaction incorporating both chemical and structural factors in the near future.

CONCLUSION

In summary, we studied the surface hydrophilicity of *Scarus persicus* scales by means of nanoscale force reconstruction. Among all the scales tested, the exposed part of the scale (Region 1) became more hydrophobic in higher humidity, while the covered part (Regions 2 and 3) tended to attract

more water. A reversed behavior was observed as the scales approached a saturated state. To the best of the authors' knowledge, this is the first reported example of observable differences in wetting behavior both between and within fish scales, as well as the first use of this force reconstruction technique to characterize a biological sample. Fish scales hold great potential for engineering applications, especially in the area of nautical vessel coatings, as their properties rely on a complex interaction of scale chemistry and morphology and the environment. Studying these interactions would increase our understanding of how nature tackles challenges that are also encountered by manufactured crafts. For example, the ability to retain mucus-like substances could allow boats with anti-biofouling coatings to reduce their coating loss over time. We believe that this work has opened the door not only to further studies in functional coatings inspired by the mucus-scale system, but also to the characterization of nanoscale wetting of complex, finely structured biomaterials.

■ ASSOCIATED CONTENT

Supporting Information

A video of the process of water condensation at Region 3 demonstrates that contact angles could not be obtained, because water filled the valleys between ridges rapidly. This material is available free of charge via the Internet at http://pubs.acs.org.

■ AUTHOR INFORMATION

Corresponding Author

*E-mail: mchiesa@masdar.ac.ae. Tel.: +971 2 810 9333.

Present Address

[‖]Department of Biological Engineering, Massachusetts Institute of Technology, Cambridge, MA 02139

Author Contributions

[§]These authors contributed equally.

Notes

The authors declare no competing financial interest.

■ ACKNOWLEDGMENTS

The authors would like to thank the Brown International Scholars Program for its support.

■ REFERENCES

(1) Bhushan, B. Bioinspired Structured Surfaces. *Langmuir* **2012**, *28*, 1698−1714.

(2) Vernerey, F. J.; Barthelat, F. On the Mechanics of Fishscale Structures. *Int. J. Solids Struct.* **2010**, *47*, 2268−2275.

(3) Yang, W.; Chen, I. H.; Gludovatz, B.; Zimmermann, E. A.; Ritchie, R. O.; Meyers, M. A. Natural Flexible Dermal Armor. *Adv. Mater.* **2013**, *25*, 31−48.

(4) Kirschner, C. M.; Brennan, A. B. Bio-Inspired Antifouling Strategies. *Annu. Rev. Mater. Res.* **2012**, *42*, 211−229.

(5) Bechert, D.; Bruse, M.; Hage, W. Experiments with Three-Dimensional Riblets as an Idealized Model of Shark Skin. *Exp. Fluids* **2000**, *28*, 403−412.

(6) Liu, X.; Zhou, J.; Xue, Z.; Gao, J.; Meng, J.; Wang, S.; Jiang, L. Clam's Shell Inspired High-Energy Inorganic Coatings with Underwater Low Adhesive Superoleophobicity. *Adv. Mater.* **2012**, *24*, 3401−3405.

(7) Zhu, D.; Ortega, C. F.; Motamedi, R.; Szewciw, L.; Vernerey, F.; Barthelat, F. Structure and Mechanical Performance of a "Modern" Fish Scale. *Adv. Eng. Mater.* **2012**, *14*, B185−B194.

(8) Lin, Y.; Wei, C.; Olevsky, E.; Meyers, M. A. Mechanical Properties and the Laminate Structure of *Arapaima gigas* Scales. *J. Mech. Behav. Biomed. Mater.* **2011**, *4*, 1145−1156.

(9) Bruet, B. J.; Song, J.; Boyce, M. C.; Ortiz, C. Materials Design Principles of Ancient Fish Armour. *Nat. Mater.* **2008**, *7*, 748−756.

(10) Shephard, K. L. Functions for Fish Mucus. *Rev.: Methods Technol. Fish Biol. Fish.* **1994**, *4*, 401−429.

(11) Chen, P.-Y.; Schirer, J.; Simpson, A.; Nay, R.; Lin, Y.-S.; Yang, W.; Lopez, M. I.; Li, J.; Olevsky, E. A.; Meyers, M. A. Predation versus Protection: Fish Teeth and Scales Evaluated by Nanoindentation. *J. Mater. Res.* **2012**, *27*, 100−112.

(12) Sudo, S.; Tsuyuki, K.; Ito, Y.; Ikohagi, T. A Study on the Surface Shape of Fish Scales. *JSME Int. J., Ser. C* **2002**, *45*, 1100−1105.

(13) Ikoma, T.; Kobayashi, H.; Tanaka, J.; Walsh, D.; Mann, S. Microstructure, Mechanical, and Biomimetic Properties of Fish Scales from Pagrus Major. *J. Struct. Biol.* **2003**, *142*, 327−333.

(14) Bhushan, B.; Jung, Y. C. Natural and Biomimetic Artificial Surfaces for Superhydrophobicity, Self-Cleaning, Low Adhesion, and Drag Reduction. *Prog. Mater. Sci.* **2011**, *56*, 1−108.

(15) Israelachvili, J. N. *Intermolecular and Surface Forces*, 3rd ed.; Academic Press: Burlington, MA, 2011.

(16) Gruebele, M.; Thirumalai, D. Perspective: Reaches of Chemical Physics in Biology. *J. Chem. Phys.* **2013**, *139*, 121701.

(17) Amadei, C. A.; Tang, T. C.; Chiesa, M.; Santos, S. The Aging of a Surface and the Evolution of Conservative and Dissipative Nanoscale Interactions. *J. Chem. Phys.* **2013**, *139*, 084708.

(18) Sader, J. E.; Jarvis, S. P. Accurate Formulas for Interaction Force and Energy in Frequency Modulation Force Spectroscopy. *Appl. Phys. Lett.* **2004**, *84*, 1801−1803.

(19) Katan, A. J.; Van Es, M. H.; Oosterkamp, T. H. Quantitative Force versus Distance Measurements in Amplitude Modulation AFM: A Novel Force Inversion Technique. *Nanotechnology* **2009**, *20*, 165703.

(20) García, R.; San Paulo, A. Attractive and Repulsive Tip-Sample Interaction Regimes in Tapping-Mode Atomic Force Microscopy. *Phys. Rev. B* **1999**, *60*, 4961−4967.

(21) Garcia, R.; San Paulo, A. Amplitude Curves and Operating Regimes in Dynamic Atomic Force Microscopy. *Ultramicroscopy* **2000**, *82*, 79−83.

(22) Santos, S.; Guang, L.; Souier, T.; Gadelrab, K.; Chiesa, M.; Thomson, N. H. A Method to Provide Rapid in Situ Determination of Tip Radius in Dynamic Atomic Force Microscopy. *Rev. Sci. Instrum.* **2012**, *83*, 043707.

(23) Amadei, C. A.; Santos, S.; Pehkonen, S. O.; Verdaguer, A.; Chiesa, M. Minimal Invasiveness and Spectroscopy-Like Footprints for the Characterization of Heterogeneous Nanoscale Wetting in Ambient Conditions. *J. Phys. Chem. C* **2013**, *117*, 20819−20825.

(24) Santos, S.; Barcons, V.; Verdaguer, A.; Font, J.; Thomson, N. H.; Chiesa, M. How Localized Are Energy Dissipation Processes in Nanoscale Interactions? *Nanotechnology* **2011**, *22*, 345401.

(25) Guzman, H. V.; Perrino, A. P.; Garcia, R. Peak Forces in High-Resolution Imaging of Soft Matter in Liquid. *ACS Nano* **2013**, *7*, 3198−3204.

(26) Liukkonen, A. Contact Angle of Water on Paper Components: Sessile Drops Versus Environmental Scanning Electron Microscope Measurements. *Scanning* **1997**, *19*, 411−415.

(27) Hikita, M.; Tanaka, K.; Nakamura, T.; Kajiyama, T.; Takahara, A. Super-Liquid-Repellent Surfaces Prepared by Colloidal Silica Nanoparticles Covered with Fluoroalkyl Groups. *Langmuir* **2005**, *21*, 7299−7302.

(28) Tang, T.-C.; Amadei, C. A.; Thomson, N. H.; Chiesa, M. Ion Exchange and DNA Molecular Dip Sticks: Studying the Nanoscale Surface Wetting of Muscovite Mica. *J. Phys. Chem. C* **2014**, *118*, 4695−4701.